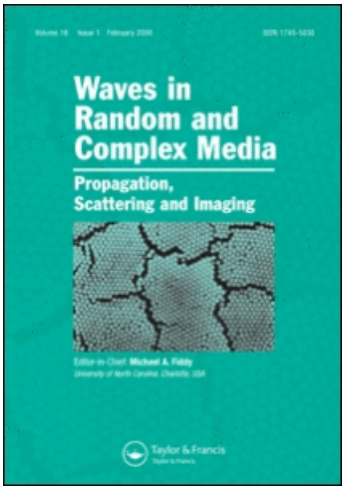

Waves in Random and Complex Media
Publication details, including instructions for authors and subscription information:
http://www.informaworld.com/smpp/title~content=t716100762

HF ground wave propagation over a curved rough sea surface

C. Bourlier[a]; G. Kubické[a]
[a] IREENA, PolyTech'Nantes-Université de Nantes, La Chantrerie, 44306 Nantes Cedex 3, France

Online publication date: 28 January 2011

To cite this Article Bourlier, C. and Kubické, G.(2011) 'HF ground wave propagation over a curved rough sea surface', Waves in Random and Complex Media, 21: 1, 23 — 43
To link to this Article: DOI: 10.1080/17455030.2010.505615
URL: http://dx.doi.org/10.1080/17455030.2010.505615

Waves in Random and Complex Media
Vol. 21, No. 1, February 2011, 23–43

Taylor & Francis
Taylor & Francis Group

HF ground wave propagation over a curved rough sea surface

C. Bourlier* and G. Kubické

IREENA, PolyTech'Nantes-Université de Nantes, La Chantrerie, Rue C. Pauc, BP 50609, 44306 Nantes Cedex 3, France

(*Received 14 April 2010; final version received 22 June 2010*)

For a vertically polarized line source, in the context of HF (3–30 MHz) ground wave propagation over a curved rough sea surface, this paper presents different asymptotic and rigorous methods to compute the attenuation function. When the Earth's curvature is taken into account, the attenuation function is expressed as a series, in which the roots of a differential equation, depending on the Airy function, must be calculated. In addition, from Taylor series expansions, different closed-form expressions can be obtained. For a smooth sea surface, the purpose of this paper is to compare these different formulations with fast rigorous numerical methods, such as the BMIA-CAG (Banded-Matrix-Iterative Approach CAnonical-Grid) and FB-SA (Forward-Backward Spectral-Acceleration) methods, based on the method of moments and originally developed for rough surfaces. These methods are especially efficient to solve a problem with huge unknowns, which is required to predict the ground wave propagation over a long surface. In addition, from a partial fraction expansion of the attenuation function in the Laplace domain, the Bremmer asymptotic expansion is extended to any order by including the surface roughness.

1. Introduction

There are many problems in communications, navigation, and applied geophysics where the system performance depends on the electromagnetic ground wave. The latter refers to the wave that propagates along the surface of the Earth such that its characteristics are mainly influenced by the profile and electrical properties of the Earth's surface. In addition, since the transmitter and receiver are close to the surface, direct and ground reflected waves cancel each other, and only surface waves can propagate.

As addressed in the reviews of Wait [1] and Collin [2] (and references therein), much theoretical work in the last century, based on asymptotic theories, was done to solve this issue. Recently, for a flat Earth, Bourlier et al. [3] thoroughly studied the ground wave propagation over a one-dimensional (1D) rough sea surface using an efficient rigorous numerical method: the method of moments combined with the BMIA-CAG [4,5] (Banded-Matrix-Iterative Approach CAnonical-Grid) approach

*Corresponding author. Email: christophe.bourlier@univ-nantes.fr

ISSN 1745–5030 print/ISSN 1745–5049 online

DOI: 10.1080/17455030.2010.505615
http://www.informaworld.com

and with the impedance boundary condition (Leontovitch approximation). In addition, they compared with the BMIA-CAG method, the closed-form asymptotic expression (the Sommerfeld solution of radiation of a vertically polarized line source above an infinite lossy half-space) of Collin [2], valid for a smooth surface, and modified by the roughness from the work of Barrick [6,7]. The comparisons were in good agreement for emitter and receiver heights small in comparison to the electromagnetic wavelength. A similar study has also been published by Toporkov et al. [8].

One of the purposes of this paper is to extend the previous work of Bourlier et al. in order to take the Earth's curvature into account in the computation of the ground wave propagation. Then, the BMIA-CAG and FB-SA (Forward-Backward Spectral-Acceleration) methods [9–11], two efficient numerical rigorous methods based on the method of moments and originally developed for rough surfaces, are used to validate different closed-form expressions of the attenuation function obtained from simplifying assumptions. In addition, in this paper, from a partial fraction expansion of the attenuation function in the Laplace domain, the Bremmer asymptotic expansion [12] is extended to any order and by including the surface roughness. This allows us to express the attenuation function as a sum of flat-Earth attenuation functions, each being characterized by their pole and residue.

The paper is organized as follows. For a 1D surface, from the work of Bremmer [12] and by assuming a parabolic profile of the Earth, Section 2 presents the integral equation satisfied by the attenuation function and different ways to solve it. For a smooth surface, Section 3 compares the resulting numerical results with that obtained from the BMIA-CAG and FB-SA methods, and an intuitive method is addressed to include the sea roughness. The last section gives concluding remarks.

2. Closed-form expressions of the attenuation function

This section presents closed-form expressions for the attenuation function of the ground wave propagation above a curved smooth 1D surface, obeying a parabolic profile and assumed to be highly conducting.

2.1. *Integral equation satisfied by the attenuation function*

For a 1D surface, we show in Appendix 1 that the integral equation satisfied by the attenuation function $F=\psi/(2\psi_i)$, in which ψ is the total field and ψ_i the incident field of a line source, is

$$F(x,z) = 1 + \frac{j\alpha}{\sqrt{\pi}} \int_0^x F(\xi, z_\xi) e^{jk_0(\mathrm{QR}+\mathrm{TQ}-\mathrm{TR})} \times \sqrt{\frac{\mathrm{TR}}{\mathrm{QR}\times\mathrm{TQ}}} \left[1 - \frac{\gamma_\xi(\xi - x) - (z_\xi - z)}{\Delta\sqrt{1+\gamma_\xi^2}\mathrm{QR}} \right] \sqrt{1+\gamma_\xi^2}\, \mathrm{d}\xi, \tag{1}$$

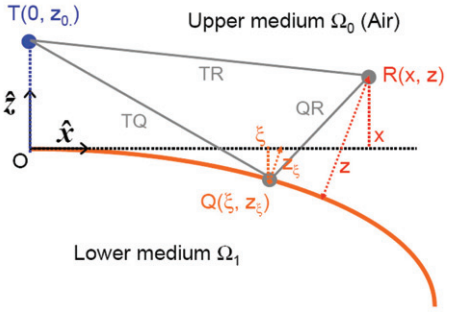

Figure 1. (Color online) Description of the geometry.

where

$$\alpha = \Delta\sqrt{\frac{jk_0}{2}} = \frac{1}{n}\sqrt{1-\frac{1}{n^2}}\sqrt{\frac{jk_0}{2}}. \tag{2}$$

The points $\mathrm{T}(0, z_0)$, $\mathrm{Q}(\xi, z_\xi)$ and $\mathrm{R}(x, z)$ give the position of the transmitter, a point on the surface of slope $\gamma_\xi = \mathrm{d}z_\xi/\mathrm{d}\xi$ and the position of the receiver, respectively (see Figure 1). The terms QR, TQ and TR are distances between two points expressed from Equation (44). The above equation is valid for $k_0\mathrm{QR} \gg 1$, $k_0\mathrm{TQ} \gg 1$ and $k_0\mathrm{TR} \gg 1$, and assumes that the surface is highly conducting ($|\Delta| \ll 1$ or $|n| \gg 1$) to apply the Leontovitch boundary condition. Δ is the surface normalized impedance, n the surface refractive index and $k_0 = 2\pi/\lambda_0$ the incident wavenumber of the upper medium assumed to be a vacuum.

The Earth's profile, z_ξ, is expressed as $z_\xi = -a^2 + \sqrt{a^2 - \xi^2}$, in which $a \approx 6378$ km is the maximum equatorial radius of the Earth. A Taylor series expansion over $\xi = 0$ and up to order 2 leads to

$$\begin{cases} z_\xi \approx -\dfrac{\xi^2}{2a} \quad \gamma_\xi \approx -\dfrac{\xi}{a} \quad \sqrt{\dfrac{\mathrm{TR}}{\mathrm{QR}\times\mathrm{TQ}}}\sqrt{1+\gamma_\xi^2} \approx \sqrt{\dfrac{x}{\xi(x-\xi)}} \\ 1 - \dfrac{\gamma_\xi(\xi - x) - (z_\xi - z)}{\sqrt{1+\gamma_\xi^2}\mathrm{QR}} \approx 1 + \dfrac{x-\xi}{2a} \quad \mathrm{QR} + \mathrm{TQ} - \mathrm{TR} \approx \dfrac{x\xi(x-\xi)}{8a^2}, \end{cases} \tag{3}$$

where the transmitter and receiver heights are assumed to be zeros ($z_0 = z = 0$). Reporting the above equations into integral Equation (1), we show that the attenuation function F is expressed as

$$F(x) = w(x)\sqrt{x}e^{\frac{jk_0x^3}{24a^2}} = \frac{\psi}{2\psi_i}, \tag{4}$$

in which the w function is expressed as

$$w(x) = \frac{e^{-\frac{jk_0x^3}{24a^2}}}{\sqrt{x}} + \frac{j\alpha}{\sqrt{\pi}}\int_0^x w(\xi)\left(1 + \frac{x-\xi}{2a\Delta}\right)\frac{e^{-\frac{jk_0(x-\xi)^3}{24a^2}}}{\sqrt{x-\xi}}\mathrm{d}\xi. \tag{5}$$

Bremmer [12] started from the scalar integral equation of a two-dimensional surface, and converted it into a single integral from a saddle point approximation [12,13]. The integral equation (5) satisfied by w and derived from a 1D surface is then exactly the same as that obtained by Bremmer (see [12], equation (1)).

For a detailed review of this issue, see also the excellent reference [14].

2.2. *Solution of the integral equation*

To solve the integral equation (5), Bremmer [12] used the Laplace transform and showed that the Laplace transform of $w(x)$, $\hat{w}(p)=\mathcal{L}[w(x)]$, is

$$\hat{w}(p)=\sqrt{\pi}\left[-j\alpha+\sqrt{p}e^{-\frac{j\pi}{6}}\frac{\mathrm{H}_{\frac{2}{3}}^{(2)}(u)}{\mathrm{H}_{\frac{1}{3}}^{(2)}(u)}\right]^{-1}, \tag{6}$$

where $\mathrm{H}_{\frac{1}{3}}^{(1)}(u)$, $\mathrm{H}_{\frac{1}{3}}^{(2)}(u)$ are the Hankel functions of order 1/3 and of the first and second kinds, respectively, and

$$u=a\left(\frac{24}{jk_0}\right)^{\frac{1}{2}}\left(\frac{p}{3}\right)^{\frac{3}{2}}. \tag{7}$$

Finally, from Equation (6) the inverse Laplace transform is derived by deforming the integration path and from the residue theorem. From Equation (4), the resulting equation is

$$F_N(x)=(k_0a)^{\frac{1}{6}}\left(\frac{2\pi jx}{a}\right)^{\frac{1}{2}}\sum_{n=1}^{n=N}\frac{e^{j(k_0a)^{\frac{1}{3}}\tau_n x/a}}{2\tau_n-\frac{1}{\delta^2}}, \tag{8}$$

where

$$\delta=\frac{j}{\Delta(ak_0)^{\frac{1}{3}}}, \tag{9}$$

and τ_n are the roots of the following equation

$$\mathrm{H}_{\frac{1}{3}}^{(1)}\left(\frac{(-2\tau)^{\frac{3}{2}}}{3}\right)+e^{-\frac{j\pi}{3}}\delta\sqrt{-2\tau}\,\mathrm{H}_{\frac{2}{3}}^{(1)}\left(\frac{(-2\tau)^{\frac{3}{2}}}{3}\right)=0. \tag{10}$$

In addition, $F(x)=\lim_{N\to\infty}F_N(x)$. For convenience, the above equation can be converted in terms of standard Airy functions $w_1(\xi)=\mathrm{Bi}(\xi)+j\mathrm{Ai}(\xi)=-2e^{-2j\pi/3}\mathrm{Ai}(e^{4j\pi/3}\xi)$ (see [15], p. 447 and [16], p. B9) as

$$w_1'(\xi)-qw_1(\xi)=0,\quad q=-\frac{1}{\delta 2^{\frac{1}{3}}},\quad \xi=2^{\frac{1}{3}}\tau. \tag{11}$$

The sum (8) converges if the roots τ_n are ordered as $-\mathrm{Im}(\tau_1)>-\mathrm{Im}(\tau_2)>\cdots>-\mathrm{Im}(\tau_N)$, where the symbol Im stands for the imaginary part, and N is the number of roots.

2.3. *Bremmer simplified form of the attenuation function*

In Equation (6) for a flat Earth ($a \to \infty$), the variable u defined from Equation (7) tends to infinity. Thus, to have a simpler form of the Laplace transform of $\hat{w}(p)$, a series expansion of the Hankel functions at infinity can be made. From [17] and for $1/|u| \to 0$, one has

$$\begin{cases} \mathrm{H}_{\frac{2}{3}}^{(2)}(u) = \sqrt{\dfrac{2}{\pi u}} e^{-j\left(u-\frac{7\pi}{12}\right)} \displaystyle\sum_{k=0}^{k=K} \frac{a_k}{u^k} + \mathrm{o}\left(\frac{1}{u^K}\right) \qquad a_k = \dfrac{1}{(2j)^k} \dfrac{\Gamma\left(k+\frac{7}{6}\right)}{k!\Gamma\left(-k+\frac{7}{6}\right)} \\ \mathrm{H}_{\frac{1}{3}}^{(2)}(u) = \sqrt{\dfrac{2}{\pi u}} e^{-j\left(u-\frac{5\pi}{12}\right)} \displaystyle\sum_{k=0}^{k=K} \frac{b_k}{u^k} + \mathrm{o}\left(\frac{1}{u^K}\right) \qquad b_k = \dfrac{1}{(2j)^k} \dfrac{\Gamma\left(k+\frac{5}{6}\right)}{k!\Gamma\left(-k+\frac{5}{6}\right)}, \end{cases} \tag{12}$$

where the symbol Γ stands for the gamma function. Substitution of Equation (12) into (6) then leads to

$$\hat{w}_K(p) \approx \sqrt{\pi} \left[-j\alpha + \sqrt{p} \frac{\sum_{k=0}^{k=K} \frac{a_k}{u^k}}{\sum_{k=0}^{k=K} \frac{b_k}{u^k}} \right]^{-1}. \tag{13}$$

In addition, since $b_0 = 1$ and $1/|u| \to 0$, from $1/(1+x) = \sum_{k=0}^{k=\infty} (-x)^k$ for $|x| < 1$, the ratio can be written as

$$\frac{\sum_{k=0}^{k=K} \frac{a_k}{u^k}}{1 + \sum_{k=1}^{k=K} \frac{b_k}{u^k}} \approx \sum_{k=0}^{k=K} \frac{a_k}{u^k} \times \underbrace{\left[\sum_{k=0}^{k=K} \left(- \sum_{k=1}^{k=K} \frac{b_k}{u^k} \right)^k \right]}_{\frac{c_k}{u^k}} + \mathrm{o}\left(\frac{1}{u^K}\right), \tag{14}$$

in which, from Equation (12),

$$\begin{cases} c_0 = 1 \qquad c_1 = -\dfrac{1}{6} \qquad c_2 = \dfrac{5}{72} \qquad c_3 = \dfrac{5j}{72} \qquad c_4 = -\dfrac{1105}{10368} \qquad c_5 = -\dfrac{565j}{2592} \\ c_6 = \dfrac{414125}{746496} \quad c_7 = \dfrac{19675j}{11664} \quad c_8 = -\dfrac{1282031525}{214990848} \quad c_9 = -\dfrac{80727925j}{3359232} \quad \ldots \end{cases} \tag{15}$$

In Equation (14), keeping the terms in $1/u^k$ up to order 3 ($K = 3$), and substituting the resulting equation into Equation (13), one has

$$\hat{w}_K(p) \approx \sqrt{\pi} \left[-j\alpha + p^{\frac{1}{2}} \left(1 - \frac{1}{6u} + \frac{5}{72u^2} + \frac{5j}{72u^3} \right) \right]^{-1}. \tag{16}$$

For $K \leq 3$, Bremmer then showed that

$$w_K(x)\sqrt{x} \approx F_{\mathrm{flat}}\left(s_0\sqrt{x}\right) + \sum_{k=1}^{k=K, K\leq 3} \delta^{3k} F_k\left(s_0\sqrt{x}\right), \tag{17}$$

where F_{flat} is the attenuation function of a flat Earth expressed as

$$F_{\mathrm{flat}}(v) = \sqrt{x}\mathcal{L}^{-1}\left(\frac{\sqrt{\pi}}{-j\alpha + \sqrt{p}}\right) = 1 - \sqrt{\pi} v e^{v^2} \mathrm{erfc}(v) \quad v = j\alpha\sqrt{x} = \sqrt{\frac{k_0 x}{2j}}\Delta. \tag{18}$$

In addition the functions $\{F_k(v)\}$ are given from Equation (34) of [12] and $s_0 = j\alpha$.

2.4. *Partial fraction expansion of the attenuation function*

In a similar way, the same derivation can be made for any order. Indeed, substitution of Equation (14) into (13) with $u=\beta s^3$ leads to

$$\hat{w}_K(p) \approx \frac{\sqrt{\pi} s^{3K-1}}{-j\alpha s^{3K-1} + \sum_{k=0}^{k=K} c_k \beta^{-k} s^{3(K-k)}}, \quad s=\sqrt{p}, \quad \beta = \frac{2a}{3}\sqrt{\frac{2}{jk_0}}. \tag{19}$$

For $K=0$, $\hat{w}_0(p) = \sqrt{\pi}/(-j\alpha + s) = \sqrt{\pi}/(-j\alpha + \sqrt{p})$, corresponding to a flat Earth. Thus, the higher orders ($K>0$) are related to the Earth's curvature like in the Bremmer approach presented in the previous subsection. In addition, since the higher degree of the numerator ($3K-1$) is smaller than the higher degree of the denominator ($3K$), for $K>0$, $\hat{w}_K(p)$ can be expanded as

$$\hat{w}_K(p) \approx \sqrt{\pi} \sum_{k=1}^{k=3K} \frac{R_k}{s-s_k}, \quad R_k = \frac{1}{\sqrt{\pi}} \lim_{s\to s_k} \hat{w}_K(s)(s-s_k), \tag{20}$$

and s_k are the roots of the polynomial of the denominator of Equation (19). In addition, Equation (20) is valid if the poles $\{s_k\}$ are simple. Thus, since $s=\sqrt{p}$, the function $\hat{w}_K(p)$ is expressed as a sum of functions of a flat Earth weighted by the residue R_k and their pole s_k. For a flat Earth ($K=0$), $s_0=j\alpha$ and $R_0=1$. As a conclusion, $w_K(x)$ is given by

$$w_K(x)\sqrt{x} \approx \begin{cases} F_{\text{flat}}\left(s_0\sqrt{x}\right) & K=0 \\ \displaystyle\sum_{k=1}^{k=3K} R_k F_{\text{flat}}\left(s_k\sqrt{x}\right) & K>0. \end{cases} \tag{21}$$

Instead of using the decomposition (14), which adds an additional restriction, Equation (13) can be applied directly. Applying the same way as previously, we show that

$$\hat{w}_K(s) \approx \frac{\sqrt{\pi}\sum_{k=0}^{k=K} b_k \beta^{K-k} s^{3(K-k)}}{\sum_{k=0}^{k=K}(-j\alpha b_k + s a_k)\beta^{K-k} s^{3(K-k)}}. \tag{22}$$

The case $K=0$ corresponds to a flat Earth. As previously, since the higher degree of the numerator ($3K$) is smaller than the higher degree of the denominator ($3K+1$), $\hat{w}_K(p)$ can be expanded as

$$\hat{w}_K(p) \approx \sqrt{\pi} \sum_{k=1}^{k=3K+1} \frac{R_k}{s-s_k}, \tag{23}$$

and s_k are the roots of the polynomial of the denominator of Equation (22). As a conclusion, for $K\geq 0$, $w_K(x)$ is given by

$$w_K(x)\sqrt{x} \approx \begin{cases} F_{\text{flat}}\left(s_0\sqrt{x}\right) & K=0 \\ \displaystyle\sum_{k=1}^{k=3K+1} R_k F_{\text{flat}}\left(s_k\sqrt{x}\right) & K>0. \end{cases} \tag{24}$$

3. Numerical results

In this section, results computed from the different formulations given from Equations:

- (8): Bremmer's rigorous solution expressed from a residues series;
- (17): Bremmer's asymptotic solution expressed from a truncated partial fraction expansion;
- (21): the solution expressed from a partial fraction expansion (first decomposition);
- (24): the solution expressed from a partial fraction expansion (second decomposition)

are compared.

The first subsection compares and studies the convergence of these different formulations, and the second subsection compares them with fast rigorous numerical methods, like the BMIA-CAG (Banded-Matrix-Iterative Approach CAnonical-Grid) and FB-SA (Forward-Backward with Spectral-Acceleration) methods.

In the following, the surface complex relative permittivity ϵ_r is assumed to be

$$\epsilon_r = \epsilon_r' + \frac{j\sigma}{2\pi f \epsilon_0} = \epsilon_r' + \frac{18j\sigma}{f(\mathrm{GHz})}, \tag{25}$$

where σ is the conductivity in S/m, and $n = \sqrt{\epsilon_r}$. In addition, $\sigma = 4\,\mathrm{S/m}$ and the real part of the relative permittivity is $\epsilon_r' = 80$, which implies that the sea complex relative permittivity is $\epsilon_r = 80 + 72j/f$, with f in GHz. For instance, for $f = 10\,\mathrm{MHz}$, $\epsilon_r = 80 + j7200 \Rightarrow \Delta = 0.00838 - j0.00829$. Moreover, the Earth's radius is assumed to be $a = 6378\,\mathrm{km}$ (maximum equatorial radius).

From Equation (4), one has

$$\left|F(x)\right| = \left|w(x)\right|\sqrt{x}. \tag{26}$$

3.1. *Comparison and convergence of the different formulations*

Equation (8) needs to compute the roots of Equation (11), τ_n. Among a number of different algorithms for determining these roots, the one described in [18] (pp. 340–343) is seen to be very accurate and valid for a wide range of frequencies and ground constants. Its principle is summarized in Appendix 2. An analytical series expansion of τ_n can be also found in [14].

Figure 2 plots the ratio $|s_k/s_0|$, the phase of s_k and $|R_k|$ versus the integer k, respectively. They are computed from the first decomposition given by Equation (21). The frequency is $f = 10\,\mathrm{MHz}$. The poles $\{s_k\}$ are ordered as $|R_0| > |R_1| > \cdots > |R_{3K}|$. Figure 3 plots the same variation but from the second decomposition given by Equation (24). If $\mathrm{Re}(s_k) \leq 0$, then the argument of $s_k, \phi_{s_k} = \arg(s_k)$, must verify $|\phi_{s_k}| \geq \pi/2$, where the symbol Re stands for the real part. As can be seen, Figures 2 and 3 present similar behavior.

Figure 4 plots the modulus $|F_K(x)|$ versus the horizontal distance x and the integer K. Panels (a), (b), (c) and (d) are obtained from Equations (21), (24), (17)

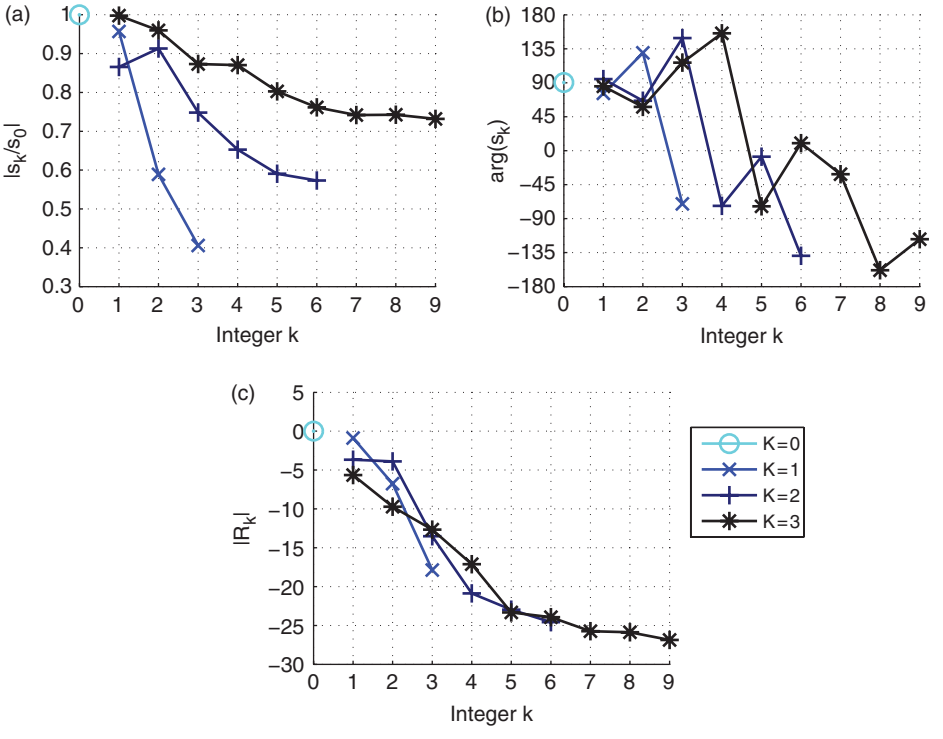

Figure 2. (Color online) (a) The ratio $|s_k/s_0|$ versus the integer k. (b) The phase of s_k versus k. (c) The residue modulus $|R_k|$ in dB scale versus the integer k. The curves are obtained from the first decomposition, corresponding to Equation (21). $f = 10$ MHz.

and (8), respectively. As K increases, panels (a), (b) and (c) show that the series diverges for large values of x, whereas panel (d) shows a very good convergence and does not converge for x close to zero. It is important to note that the integers N and K have different physical interpretations.

The formulations based on the partial fraction decomposition assume that the parameter $|u| = |\beta p^{3/2}| > 1$, which implies that $|\beta| > |p|^{-3/2}$. The Laplace variable p is related to the inverse of the horizontal distance x, leading to $x < |\beta|^{2/3} = x_p$. This value is shown in Figure 4(a) and (b) from the vertical dashed line. As we can see, for $x > x_p$ the results differ according to the value of $K > 0$.

As $x \to \infty$, Equation (18) tends to zero if the real part of the pole is negative. For instance, for a flat Earth, $s_0 = j\alpha = -0.0000212 + j0.00381$. In Figures 2 and 3, the real part of the pole can be positive ($|\phi_{s_k}| < \pi/2$), which implies, for large distance x, that the series diverges, as shown in Figure 4(a) and (b). If we omit these poles in the computation of the series, then the series converges, but the results for x close to zero are unphysical. In conclusion, these poles must be included and these kinds of decomposition, expressed as a sum of flat-Earth attenuation functions, can be applied only for short distances, typically for $x < 2x_p = 111$ km (see Figure 5) for $f = 10$ MHz.

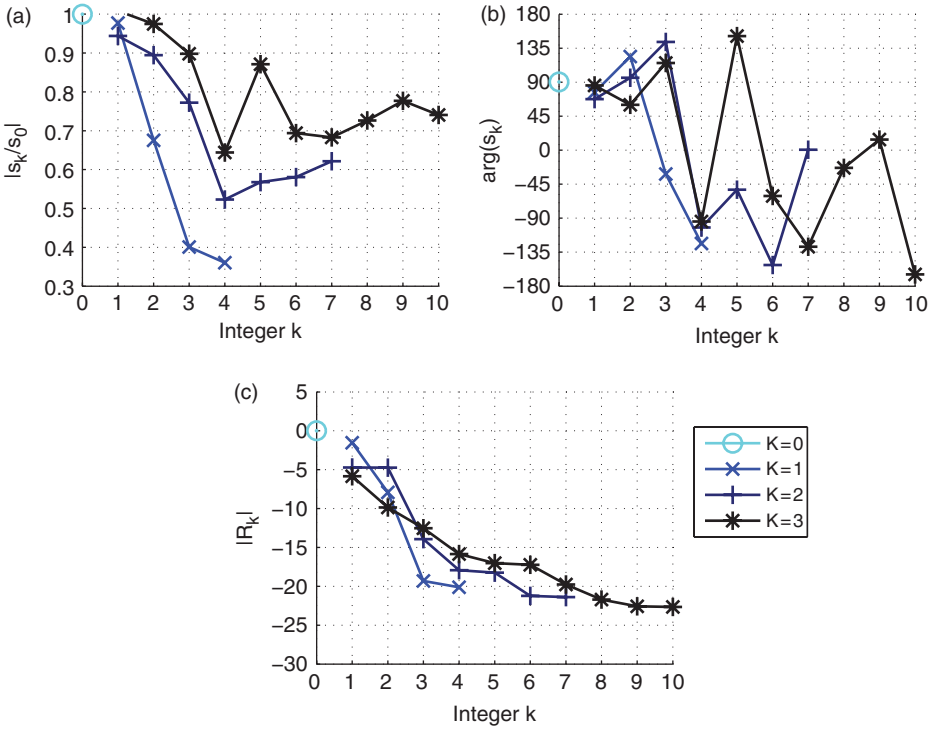

Figure 3. (Color online) Same as in Figure 2 but for the second decomposition, corresponding to Equation (24).

In the following, for the Bremmer formulation, $K=2$, whereas for the first and second decompositions, $K=3$.

For the different formulations, Figure 5 plots the modulus $|F_K(x)|$ versus the horizontal distance x. The legends '1st Dec', '2nd Dec', 'Bremmer Dec' and 'Bremmer Res' mean that the curves are obtained from Equations (21), (24), (17) and (8), respectively. As we can see, the results are similar for $x < 2x_p = 111$ km, and above this value, the results diverge, except those computed from the residues series.

Figures 6 and 7 plot, respectively, the same variations as in Figures 4 and 5 but for $f=20$ MHz. As expected, as the frequency increases, the signal strength decreases more rapidly with the distance x. As for the case $f=10$ MHz, for $x < 2x_p$, the different curves in Figure 7 give similar levels, meaning that the condition $x < 2x_p = 2|\beta|^{2/3}$ seems to be a good criterion for the domain of validity of the decomposition of the attenuation function as the sum of flat-Earth attenuation functions.

3.2. *Comparison with fast rigorous numerical methods*

This section applies two rigorous fast methods based on the integral equations, which allow us to consider a very long surface. Indeed, to exhibit the ground wave,

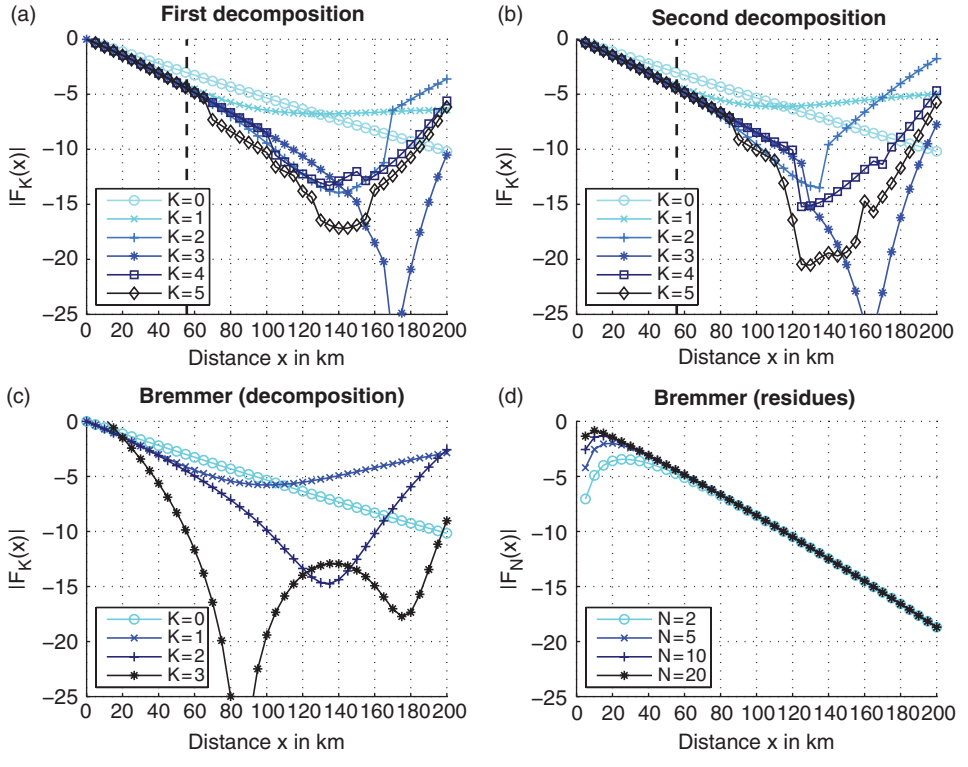

Figure 4. (Color online) Modulus $|F_K(x)|$ in dB scale versus the horizontal distance x and the integer K. $f = 10$ MHz.

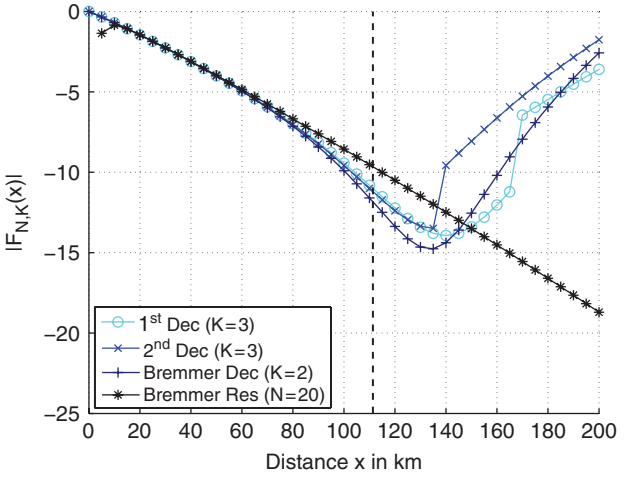

Figure 5. (Color online) Modulus $|F_K(x)|$ in dB scale versus the horizontal distance x.

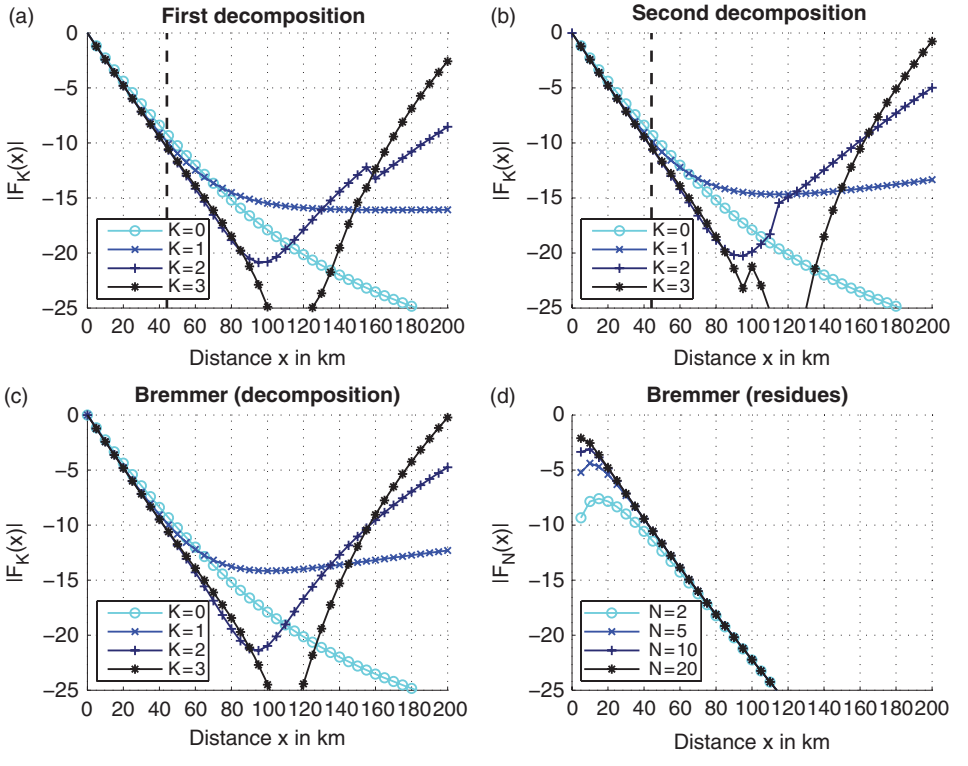

Figure 6. (Color online) Same as in Figure 4 but for $f = 20$ MHz.

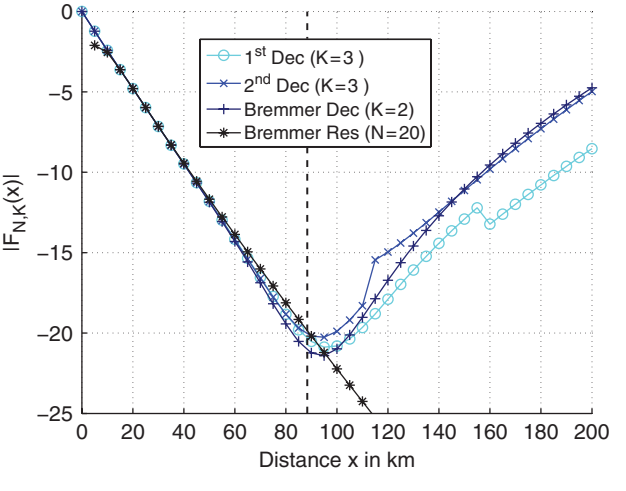

Figure 7. (Color online) Same as in Figure 5 but for $f = 20$ MHz.

which propagates near the surface over a very long distance from the transmitter, the surface must be very long, typically, a few hundred kilometers. For a frequency of the order of 10 MHz ($\lambda_0 = 30$ m) and with a sampling step of $\lambda_0/10 = 3$ m, the number of unknowns on the surface must then be greater than $N_i = 100{,}000$. The principle of these methods is not to invert the impedance matrix $\bar{\mathbf{Z}}$ but to replace $\bar{\mathbf{Z}}^{-1}\mathbf{b}$, in which the vector $\mathbf{b}$ is related to the incident field, by a succession of matrix-vector products. For more details, see [9,10,19,20] for the FB-SA and [4,5,21,22] for the BMIA-CAG. Since the surface is assumed to be highly conducting ($|n| \gg 1$), the IBC (Impedance Boundary Condition, also named the Leontovitch boundary condition) approximation can be applied. For the TM polarization, this leads to $\partial\psi(\mathbf{r}')/\partial n_s = -j\Delta k_0 \psi(\mathbf{r}')$ on the surface, where $\psi(\mathbf{r}')$ is the field on the surface and $\partial\psi(\mathbf{r}')/\partial n_s$ is the normal derivative of the field on the surface.

The scattered field is derived from the field $\psi(\mathbf{r}')$, computed either from BMIA-CAG or the FB-SA, and its normal derivative on the surface, $\partial\psi(\mathbf{r}')/\partial n_s = -j\Delta k_0 \psi(\mathbf{r}')$, by applying Huygens' principle, defined as

$$\psi_s(\mathbf{r}) = \int_S \left[\frac{\partial g_0(\mathbf{r}', \mathbf{r})}{\partial n_s} \psi(\mathbf{r}') - \frac{\partial \psi(\mathbf{r}')}{\partial n_s} g_0(\mathbf{r}', \mathbf{r}) \right] \mathrm{d}S'. \tag{27}$$

The attenuation function is then computed from ψ_s as

$$F(\mathbf{r}) = \frac{\psi_s(\mathbf{r}) + \psi_i(\mathbf{r})}{2\psi_i(\mathbf{r})} = F(x, z), \tag{28}$$

where the incident field $\psi_i(\mathbf{r})$ is defined as

$$\psi_i(\mathbf{r}) = g_0(\mathbf{r}, \mathbf{r}_0) = \frac{j}{4} H_0^{(1)}\left(k_0 \sqrt{(x - x_0)^2 + (z - z_0)^2} \right). \tag{29}$$

The emitter is located at $(x_0, z_0) = (0, 5)$ m and the surface length is $L = N_i\lambda_0/10$ ($x \in [-L/2; L/2]$), since the sampling step is $\lambda_0/10$. It should be noted that $x_{\max} = \max(x) = N_i\lambda_0/20$.

3.2.1. *Smooth sea surface*

Firstly, a smooth sea surface is considered ($\sigma_z = 0$, surface height standard deviation).

Figure 8(a) plots the modulus of the attenuation function versus x. Figure 8(b) plots the ratio $F(x)/F_1(x)$ in dB scale versus x, in which F_1 is computed from Equation (8). $f = 10$ MHz and the receiver height is $z = 5$ m. In the legend, the label 'BMIA-CAG' means that the results are computed from the BMIA-CAG, whereas the label 'FB-SA' means that the results are computed from the FB-SA. In addition, the label 'Cir' means that the Earth has a circular profile ($z_\xi = -a + \sqrt{a^2 - \xi^2}$), instead of a parabolic profile ($z_\xi \approx -\xi^2/(2a)$).

For the BMIA-CAG, since its convergence is related to $\Delta z = \max(z) - \min(z)$, the maximum distance is 49 km ($N_i = 2^{15} = 32{,}768$), corresponding to $\Delta z = 6.3\lambda_0$. Above this distance, the BMIA-CAG diverges. The strong interaction band matrix is $N_{s,\mathrm{BMIA}} = 3$ and the number of terms retained in the series expansion of the

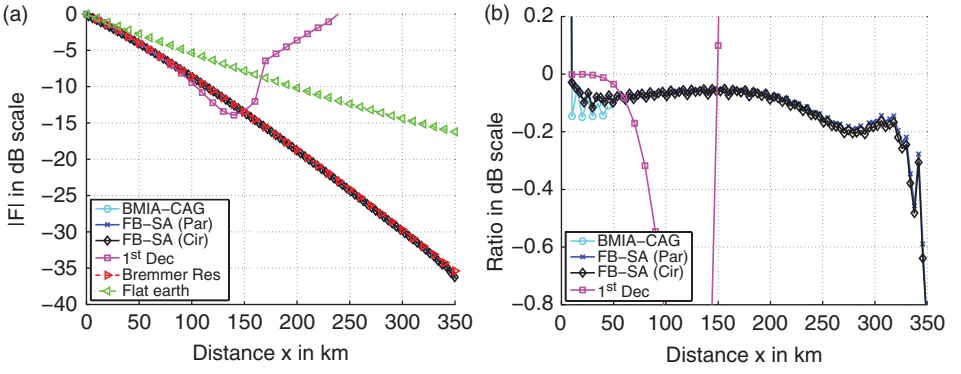

Figure 8. (Color online) (a) $|F(x)|$ in dB scale versus x. (b) The ratio $F(x)/F(x)_{\text{Equation (8)}}$ in dB scale versus x. Case of a smooth sea surface. $f = 10$ MHz and the receiver height is $z = 5$ m.

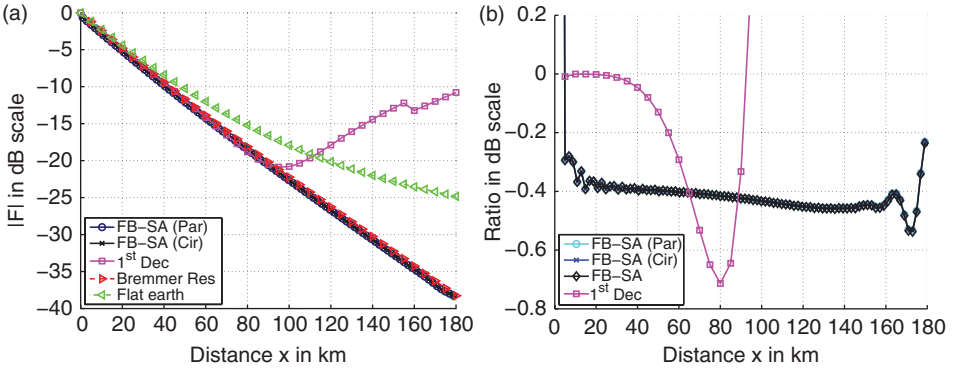

Figure 9. (Color online) Same as in Figure 8 but for $f = 20$ MHz.

impedance matrix elements of the weak interactions is $P_{\text{BMIA}} = 2$. Some numerical tests, not reported here, on the convergence of BMIA-CAG versus $\{P_{\text{BMIA}}, N_{s,\text{BMIA}}\}$ have been done. Unfortunately, even with large values of x_s and P_{BMIA}, the BMIA-CAG does not converge. A detailed analysis on the convergence of the BMIA-CAG is reported in [22].

In contrast, the FB-SA works well for longer distances. Indeed, $N_i = 2^{18} = 262,144 \Rightarrow x_{\max} = 393$ km, and the distance of the strong interaction is $x_{d0} = 50\lambda_0 = 1500$ m. Since the length x_{d0} is much greater than one, N_i cannot exceed 2^{18} due to the memory requirement to store the matrix elements of the strong interactions. A means to avoid this drawback is to compute them at each iteration of the FB but the computing time increases significantly. Figure 9 plots the same variation as in Figure 8 but for $f = 20$ MHz.

For x close to zero, the ratio increases significantly because Equation (8) is only valid in far field. In addition, for large values of x, the agreement is less good, which

can be attributed to the edge effect (finite length of the surface). Otherwise, a good agreement is obtained between the FB-SA, BMIA-CAG and Bremmer formulations.

Figures 8 and 9 show also that the Earth's profile can be modeled as a parabolic profile because the results computed from a circular profile are exactly the same. As expected, the results obtained from the first decomposition are only valid for small distances. In comparison to a flat Earth, the curvature effect implies a significant decrease of the attenuation function and this deviation, according to a flat Earth, increases with the distance and decreases as the frequency increases.

3.2.2. *Rough sea surface*

In this subsection, a rough sea surface is considered. The rough surface height is assumed to be a Gaussian stationary stochastic process with zero mean value, and the height spectrum obeys the Elfouhaily et al. hydrodynamic spectrum [23], in which the key parameter is the wind speed u_{10} at 10 meters above the sea surface. From an electromagnetic point of view, in the HF band, since the ratio σ_z/λ_0 is much smaller than one, the surface is slightly rough. From the Elfouhaily spectrum, Bourlier et al. [24] showed that the height standard deviation is $\sigma_z \approx 6.29 \times 10^{-3} u_{10}^{2.02}$. For instance for $u_{10} = 10\,\text{m/s}$ (Beaufort scale 6–7), $\sigma_z = 0.63\,\text{m}$, which implies that the ratio $\sigma_z/\lambda_0 \in [0.021;\ 0.042]$ for $f \in [10;\ 20]$ MHz.

By using a spectral method, several independent surfaces (but with the same Gaussian process and the same height spectrum) are generated. For each surface numbered p, the field ψ_p and its normal derivative $\partial\psi_p/\partial n_s$ are computed, and then from Equations (27), (28) and (29) the scattered field $\psi_{s,p}$ and the function F_p are computed. The average of F, denoted as $\langle F \rangle$, is then obtained from

$$\langle F \rangle = \frac{1}{N_r} \sum_{p=1}^{p=N_r} F_p, \tag{30}$$

where N_r is the number of realizations.

From an asymptotic perturbative theory and assuming a *flat* (the Earth's curvature is neglected) rough surface, Ishimaru et al. [25] showed that the coherent attenuation function $\langle F \rangle$ keeps the same form as that of a smooth surface, but with a new surface normalized impedance, Δ^{rough}, as functions of the smooth surface normalized impedance, $\Delta^{\text{flat}} = \Delta$, and of the sea roughness spectrum. In other words, $\Delta^{\text{rough}} \approx \Delta^{\text{flat}}(1 + a + jb)$, where $(a,\ b) \in \mathbb{R}^2$.

Assuming a *flat* rough sea surface, from the BMIA-CAG, Bourlier et al. [3] investigated several methods to compute the real numbers a and b. They then showed that $a > 0$ and is proportional to u_{10}^2, whereas $b < 0$ and $|b/a| \ll 1$. In addition, they compared a and b with that obtained from an analytical approach developed by Barrick [6,7] and based on an asymptotic perturbative theory. A good agreement is then obtained between both methods.

To our knowledge, the approach developed for a *flat* rough surface has not been generalized to the case of a *curved* rough surface. Thus, to solve this issue, the method used to take the roughness into account for a *flat* rough surface is assumed to be valid for a *curved* rough surface.

Figure 10(a) plots the modulus of the attenuation function in dB scale versus x and u_{10}. Figure 10(b) plots the ratio $F(x)/F(x)_{\text{FB-SA}}$ in dB scale versus x and u_{10}. $f=10\,\text{MHz}$ and the receiver height is $z=5\,\text{m}$. In the legend, the label 'Bremmer Res+' means that the results are computed from Equation (8) (Bremmer's rigorous solution expressed in terms of a residues series), in which the surface normalized impedance, $\Delta^{\text{flat}}=\Delta$, is substituted for Δ^{rough} computed from the work of Barrick [6,7]. Figure 11 shows the same variation as in Figure 10 but for $f=20\,\text{MHz}$.

As the wind speed increases, the attenuation function modulus decreases as observed for a flat rough sea surface. In addition, a satisfactory agreement is observed between the reference method (FB-SA) and the analytical one, which validates the proposed intuitive approach. Nevertheless, as the wind increases the difference slightly increases. Indeed, as the surface roughness increases, the perturbative approach developed by Barrick becomes questionable. For example, for $u_{10}=\{5,10\}\,\text{m/s}$, $k_0\sigma_z=\{0.034,0.138\}$ for $f=10\,\text{MHz}$, whereas $k_0\sigma_z=\{0.068,0.276\}$ for $f=20\,\text{MHz}$.

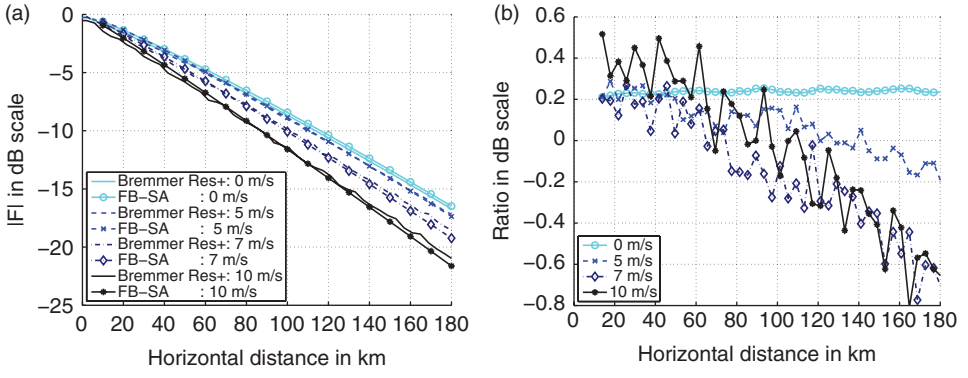

Figure 10. (Color online) (a) $|F(x)|$ in dB scale versus x. (b) The ratio $F(x)/F(x)_{\text{FB-SA}}$ in dB scale versus x. $f=10\,\text{MHz}$, the receiver height is $z=5\,\text{m}$ and the surface is rough.

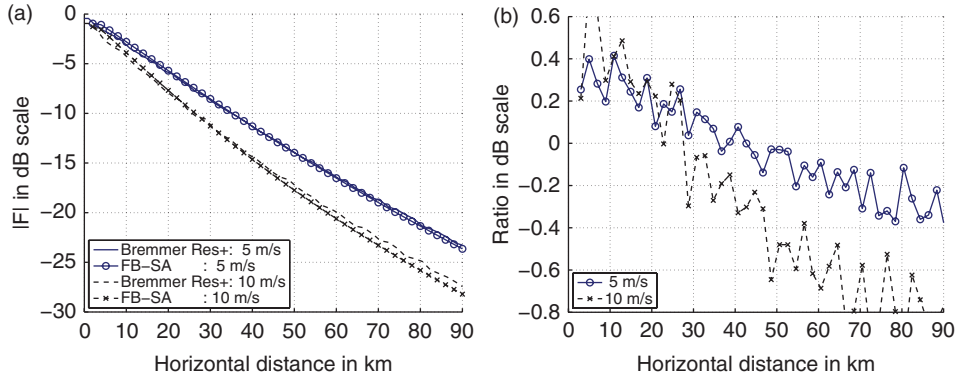

Figure 11. (Color online) Same as in Figure 10 but for $f=20\,\text{MHz}$.

This can explain why the ratio in Figure 11 is greater, in absolute value, than that in Figure 10.

4. Conclusion

For a vertically polarized line source in the HF band, analysis of the propagation over one-dimensional highly conducting curved rough sea surfaces was investigated from an efficient rigorous numerical method: the method of moments combined with the FB-SA approach. The ground wave is then exhibited for flat and curved rough sea surfaces. In addition, the numerical results are compared with Bremmer's rigorous solution expressed as a residues series, valid for a curved *smooth* surface of parabolic profile, in which the surface normalized impedance is substituted for a modified surface normalized impedance to include the surface roughness and computed from the work of Barrick. Comparisons then showed a good agreement between the FB-SA results and Bremmer's results, which validates Bremmer's rigorous solution combined with the work of Barrick.

For short distances, typically smaller than $x_p = \eta|\beta|^{3/2} = \eta(\frac{8a^2}{9k_0})^{1/3}$, where η ranges approximately from 1 to 2, this paper also showed that the attenuation function can be approximated as a sum of flat-Earth attenuation functions, each being characterized by their pole and residue. In addition, for $x \in [0; x_p]$, the Bremmer asymptotic solution given by Equation (17) can be applied.

In this paper, the emitter (z_0) and receiver (z) heights are assumed to be zeros in the Bremmer solution. For non-zeros heights, Equation (8) must be substituted for [1]

$$F_N(x) = (k_0a)^{\frac{1}{6}}\left(\frac{2\pi jx}{a}\right)^{\frac{1}{2}}\sum_{n=1}^{n=N} G_n(\nu_0)G_n(\nu)\frac{e^{j(k_0a)^{\frac{1}{3}}\tau_n x/a}}{2\tau_n - \frac{1}{\delta^2}}, \tag{31}$$

where

$$G_n(\nu) = \frac{w_1(\tau_n - \nu)}{w_1(\tau_n)}, \quad \nu_0 = \frac{k_0z_0}{(k_0a)^{1/3}}, \quad \nu = \frac{k_0z}{(k_0a)^{1/3}}, \tag{32}$$

in which G_n is a 'height-gain' function.

For small values of ν, we can show that

$$\begin{aligned} G_n(\nu) &= 1 - \nu\frac{w_1'(\tau_n)}{w_1(\tau_n)} + \nu^2\frac{w_1''(\tau_n)}{2w_1(\tau_n)} + \mathcal{O}(\nu^3) \\ &= 1 - j(k_0z)\Delta + \tau_n\frac{(k_0z)^2}{(k_0a)^{2/3}} + \mathcal{O}(\nu^3), \end{aligned} \tag{33}$$

since $w_1'(\xi_n) - qw_1(\xi_n) = 0$ with $\xi_n = 2^{1/3}\tau_n$ and $w_1''(\xi) - \xi w_1(\xi) = 0\ \forall\xi$. Thus, up to first order, $G_n(\nu)G_n(\nu_0) \approx 1 - jk_0(z + z_0)\Delta$. For instance, with $f = 10\,\text{MHz}$ and $z = z_0 = 5\,\text{m}$, $G_n(\nu)G_n(\nu_0) \approx -0.15$ dB, which approximately corresponds to the mean value in Figure 8(b). For $f = 20\,\text{MHz}$, $G_n(\nu)G_n(\nu_0) \approx -0.42$ dB, which approximately corresponds to the mean value in Figure 9(b).

In addition, the atmosphere is assumed to be homogeneous, meaning that the air refractive index is assumed to be constant and equals unity. For mean meteorological conditions, a simple means to treat an inhomogeneous atmosphere is to replace the Earth's radius a by an effective radius $a_e = Ka$, where $K = 4/3$ [18].

In this paper, the sea surface is assumed to be homogeneous, meaning that the surface permittivity is independent of the surface abscissa (no islands, for instance). This issue is currently under investigation for a flat [26] and curved Earth.

Acknowledgements

The authors would like to thank the anonymous reviewers for their useful comments.

References

[1] J.R. Wait, *The ancient and modern history of EM ground-wave propagation*, IEEE Ant. Prop. Mag. 40 (1998), pp. 7–39.
[2] R.E. Collin, *Hertzian dipole radiating over a lossy Earth or sea: Some early and late 20th-century controversies*, IEEE Ant. Prop. Mag. 46 (2004), pp. 64–79.
[3] C. Bourlier, G. Kubické, and Y. Brelet, *Rigorous prediction of the ground wave above flat and rough highly-conducting one-dimensional sea surfaces in VHF band*, IEEE Trans. Antennas Propagat. PP (2010), DOI: 10.1109/TAP.2010.2090453.
[4] L. Tsang, C.H. Chang, and H. Sangani, *A Banded Matrix Iterative Approach to Monte Carlo simulations of scattering of waves by large scale random rough surface problems: TM case*, Electron. Lett. 29 (1993), pp. 1666–1667.
[5] L. Tsang, C.H. Chang, H. Sangani, A. Ishimaru, and P. Phu, *A Banded Matrix Iterative Approach to Monte Carlo simulations of large scale random rough surface scattering: TE case*, J. Electromagn. Waves Appl. 29 (1993), pp. 1185–1200.
[6] D.E. Barrick, *Theory of HF and VHF propagation across the rough sea, 1: The effective surface impedance for a slightly rough highly conducting medium at grazing incidence*, Radio Sci. 6 (1971), pp. 517–526.
[7] D.E. Barrick, *Theory of HF and VHF propagation across the rough sea, 2: Application to HF and VHF propagation above the sea*, Radio Sci. 6 (1971), pp. 527–533.
[8] J.V. Toporkov and M.A. Sletten, *Numerical study of wide-band low-grazing HF clutter from ocean-like surfaces*, in *IEEE Antennas and Propagation Society International Symposium*, Vol. 1A, Washington, DC, 2005, pp. 388–391.
[9] D. Holliday, L.L. DeRaad Jr, and G.J. St-Cyr, *Forward–backward: a new method for computing low-grazing angle scattering*, IEEE Trans. Ant. Prop. 44 (1995), pp. 1199–1206.
[10] H.T. Chou and J.T. Johnson, *A novel acceleration algorithm for the computation of scattering from rough surfaces with the Forward-Backward method*, Radio Sci. 33 (1998), pp. 1277–1287.
[11] D. Torrungrueng, J.T. Johnson, and H.T. Chou, *Some issues related to the novel spectral acceleration method for the fast computation of radiation/scattering from one-dimensional extremely large scale quasi-planar structures*, Radio Sci. 37 (2002), pp. 1–20.
[12] H. Bremmer, *Applications of operational calculus to ground-wave propagation, particularly for long waves*, IRE Trans. Antennas. Propagat. 6 (1958), pp. 267–272.
[13] G.A. Hufford, *An integral equation approach to the problem of wave propagtion over an irregular surface*, Quart. J. Appl. Math. IX (1951), pp. 391–404.

[14] N.A. Logan and K.S. Yee, *A mathematical model for diffraction by convex surfaces*, in *Electromagnetic Waves*, R.E. Langer, ed., University of Wisconsin Press, Madison, 1962.
[15] M. Abromowitz and I.A. Stegun, *Handbook of Mathematical Functions*, Dover, New York, 1972.
[16] J.C.P. Miller, *Mathematical Tables Part Volume-B: The Airy Integral*, British Association, University Press Cambridge, Cambridge, 1946, pp. B1–B56.
[17] I.S. Gradshteyn and L.M. Ryzbik, *Table of Integrals, Series and Products*, 6th ed., Academic Press, New York, 2000.
[18] J. Galejs, *Terresterial Propagation of Long Electromagnetic Waves*, Pergamon Press, New York, 1972.
[19] N. Déchamps and C. Bourlier, *Electromagnetic scattering from a rough layer: Propagation-Inside-Layer Expansion method combined to the Forward–Backward Novel Spectral Acceleration*, IEEE Trans. Antennas Propagat. 55 (2007), pp. 3576–3586.
[20] C. Bourlier, G. Kubické, and N. Déchamps, *A fast method to compute scattering by a buried object under a randomly rough surface: PILE combined with FB-SA*, J. Opt. Soc. Am. A 25 (2008), pp. 891–902.
[21] N. Déchamps and C. Bourlier, *Electromagnetic scattering from a rough layer: Propagation-Inside-Layer Expansion method combined to an updated BMIA/CAG approach*, IEEE Trans. Antennas Propagat. 55 (2007), pp. 2790–2802.
[22] J.T. Johnson, *On the canonical grid method for two dimensional scattering problems*, IEEE Trans. Antennas Propagat. 46 (1998), pp. 297–302.
[23] T. Elfouhaily, B. Chapron, K. Katsaros, and D. Vandermark, *A unified directional spectrum for long and short wind-driven waves*, J. Geophys. Res. 102 (1997), pp. 781–796.
[24] C. Bourlier and G. Berginc, *Microwave analytical backscattering models from randomly rough anisotropic sea surface comparison with experimental data in C and Ku bands*, Prog. Electromag. Res. 37 (2002), pp. 31–78.
[25] A. Ishimaru, J.D. Rockway, Y. Kuga, and S.-W. Lee, *Sommerfeld and Zenneck wave propagation for a finitely conducting one-dimensional rough surface*, IEEE Trans. Antennas Propagat. 48 (2000), pp. 1475–1484.
[26] C. Bourlier and G. Kubické, *Ground wave propagation along an inhomogeneous rough surface in the HF band: Millington effect for a flat Earth*, accepted (2010), to appear in IEEE Trans. Geo. Remote Sens., paper no. TGRS-2010-00090.R1.
[27] L. Tsang, J.A. Kong, K.-H. Ding, and C.O. Ao, *Scattering of Electromagnetics Waves: Numerical Simulations*, Wiley Interscience, New York, 2001.

Appendix 1. Integral equation verified by the attenuation function

For a one-dimensional surface, the total field $\psi(\mathbf{r})$ and its normal derivative $\partial\psi(\mathbf{r})/\partial n_s$ on the surface satisfies, for $\mathbf{r}' \in (\Omega_0 \cup S)$ (upper medium Ω_0 plus surface S), the following integral equation [27]

$$\psi(\mathbf{r}') = \psi_i(\mathbf{r}') + \int_S \left[\psi(\mathbf{r}) \frac{\partial g_0(\mathbf{r},\mathbf{r}')}{\partial n_s} - \frac{\partial \psi(\mathbf{r})}{\partial n_s} g_0(\mathbf{r},\mathbf{r}') \right] \mathrm{d}S. \tag{34}$$

The scalar Green function of the upper medium is defined as $g_0 = g(\mathbf{r},\mathbf{r}') = \frac{j}{4} H_0^{(1)}(k_0 \|\mathbf{r}-\mathbf{r}'\|)$ and $\psi_i(\mathbf{r}')$ is the incident field illuminating the surface. The function $H_0^{(1)}$ is the Hankel function of zeroth order and of the first kind and $k_0 = 2\pi/\lambda_0$ is the incident

wavenumber. $\mathbf{r} = x\hat{\mathbf{x}} + z\hat{\mathbf{z}} = (x, z)$ is a point on the surface and $\mathbf{r}' = x'\hat{\mathbf{x}} + z'\hat{\mathbf{z}} = (x', z')$ is the observation point. $\hat{\mathbf{x}}$ and $\hat{\mathbf{z}}$ are unitary vectors in Cartesian coordinates. In Equation (34), the Cauchy principal value of the integral, defined as $\mathbf{r} = \mathbf{r}'$, is $\psi(\mathbf{r}')/2$. Thus, for $\mathbf{r}' \in \Omega_0$, Equation (34) becomes

$$\frac{\psi(\mathbf{r}')}{2} = \psi_i(\mathbf{r}') + \fint_S \left[\psi(\mathbf{r}) \frac{\partial g_0(\mathbf{r}, \mathbf{r}')}{\partial n_s} - \frac{\partial \psi(\mathbf{r})}{\partial n_s} g_0(\mathbf{r}, \mathbf{r}') \right] \mathrm{d}S. \tag{35}$$

Since the surface is assumed to be highly conducting ($|n| \gg 1$), the IBC (Impedance Boundary Condition, also named the Leontovitch boundary condition) approximation can be applied. This leads, on the surface for the TM polarization, to $\partial\psi(\mathbf{r})/\partial n_s = -j\Delta k_0 \psi(\mathbf{r})$, where Δ is the surface normalized impedance defined as $\Delta = \sqrt{1 - 1/n^2}/n$, in which n is the refractive index. The only unknown is now the field $\psi(\mathbf{r})$ and from Equation (35), one obtains

$$\frac{\psi(\mathbf{r}')}{2} = \psi_i(\mathbf{r}') + \fint_S \psi(\mathbf{r}) \left[\frac{\partial g_0(\mathbf{r}, \mathbf{r}')}{\partial n_s} + j\Delta k_0 g_0(\mathbf{r}, \mathbf{r}') \right] \mathrm{d}S, \tag{36}$$

where

$$\frac{\partial g_0(\mathbf{r}, \mathbf{r}')}{\partial n_s} = \nabla_{\mathbf{r}} g_0(\mathbf{r}, \mathbf{r}') \cdot \hat{\mathbf{n}}_s = -\frac{jk_0}{4} \frac{H_1^{(1)}(k_0 \|\mathbf{r} - \mathbf{r}'\|)}{\|\mathbf{r} - \mathbf{r}'\|} (\mathbf{r} - \mathbf{r}') \cdot \hat{\mathbf{n}}_s, \tag{37}$$

where $\hat{\mathbf{n}}_s = (-\gamma\hat{\mathbf{x}} + \hat{\mathbf{z}})/\sqrt{1 + \gamma^2}$ is the unitary vector normal to the surface at the point $\mathbf{r}$, in which $\gamma = \mathrm{d}z/\mathrm{d}x$ is the surface slope.

Assuming that $k_0 \|\mathbf{r} - \mathbf{r}'\| \gg 1$, the Green function can be expanded as

$$g_0(\mathbf{r}, \mathbf{r}') = g_0^{\infty}(\mathbf{r}, \mathbf{r}') = \frac{j}{4} \sqrt{\frac{2}{\pi k_0 \|\mathbf{r} - \mathbf{r}'\|}} e^{j(k_0 \|\mathbf{r} - \mathbf{r}'\| - \pi/4)}, \tag{38}$$

and since $H_1^{(1)}(u) \approx -jH_0^{(1)}(u)$ for $u \gg 1$, one obtains

$$\frac{\partial g_0(\mathbf{r}, \mathbf{r}')}{\partial n_s} = jk_0 g_0^{\infty}(\mathbf{r}, \mathbf{r}') \frac{\mathbf{r} - \mathbf{r}'}{\|\mathbf{r} - \mathbf{r}'\|} \cdot \hat{\mathbf{n}}_s. \tag{39}$$

Substitution of Equations (38) and (39) into Equation (36) then leads to

$$\frac{\psi(\mathbf{r}')}{2} = \psi_i(\mathbf{r}') + jk_0 \fint_S \psi(\mathbf{r})\, g_0^{\infty}(\mathbf{r}, \mathbf{r}') \left[\Delta\sqrt{1 + \gamma^2} - \frac{\gamma(x - x') - (z - z')}{\sqrt{(x - x')^2 + (z - z')^2}} \right] \mathrm{d}x, \tag{40}$$

where $\mathrm{d}S = \mathrm{d}x\sqrt{1 + \gamma^2}$.

For more clarity, the points $\mathrm{T}(0, z_0)$, $\mathrm{Q}(\xi, z_\xi)$ and $\mathrm{R}(x, z)$ are defined, and stand for the position of the transmitter, a point on the surface and the position of the receiver, respectively (see Figure 1). Assuming that $k_0\mathrm{QR} \gg 1$, with the new notations the above equation becomes

$$\frac{\psi(\mathrm{R})}{2} = \psi_i(\mathrm{R}) + jk_0 \fint_S \psi(\mathrm{Q})\, g_0^{\infty}(\mathrm{QR}) \left[\Delta\sqrt{1 + \gamma^2} - \frac{\gamma(\xi - x) - (z_\xi - z)}{\mathrm{QR}} \right] \mathrm{d}\xi, \tag{41}$$

where QR is the distance between the points Q and R.

The attenuation function is defined as $\psi = 2\psi_i F$. Substituting this equation into (41), and dividing by $\psi_i(\mathrm{R})$, one obtains for $\psi_i(\mathrm{R}) = g_0^{\infty}(\mathrm{TR})$ with $k_0\mathrm{TR} \gg 1$

$$F(\mathrm{R}) = 1 + j2k_0 \fint_S F(\mathrm{Q}) \frac{g_0^{\infty}(\mathrm{QR})\, g_0^{\infty}(\mathrm{TQ})}{g_0^{\infty}(\mathrm{TR})} \left[\Delta\sqrt{1 + \gamma^2} - \frac{\gamma(\xi - x) - (z_\xi - z)}{\mathrm{QR}} \right] \mathrm{d}\xi. \tag{42}$$

The use of Equation (38) then leads to

$$F(x,z) = 1 + \frac{j}{\sqrt{\pi}} \int_0^x F(\xi, z_\xi) \alpha e^{jk_0(\mathrm{QR}+\mathrm{TQ}-\mathrm{TR})} \times \sqrt{\frac{\mathrm{TR}}{\mathrm{QR} \times \mathrm{TQ}}} \left[1 - \frac{\gamma_\xi(\xi - x) - (z_\xi - z)}{\Delta \sqrt{1+\gamma_\xi^2}\mathrm{QR}} \right] \sqrt{1+\gamma_\xi^2}\, \mathrm{d}\xi, \tag{43}$$

where $\alpha(\xi) = \Delta(\xi)\sqrt{jk_0/2}$ and $\gamma_\xi = \gamma(\xi)$. Moreover,

$$\begin{cases} \mathrm{QR} = \sqrt{(\xi - x)^2 + (z_\xi - z)^2)} \\ \mathrm{TQ} = \sqrt{\xi^2 + (z_\xi - z_0)^2} \\ \mathrm{TR} = \sqrt{x^2 + (z - z_0)^2}. \end{cases} \tag{44}$$

Appendix 2. Algorithm to compute the roots of Equation (11)

This appendix presents a simple and efficient algorithm [18] to compute the roots of Equation (11).

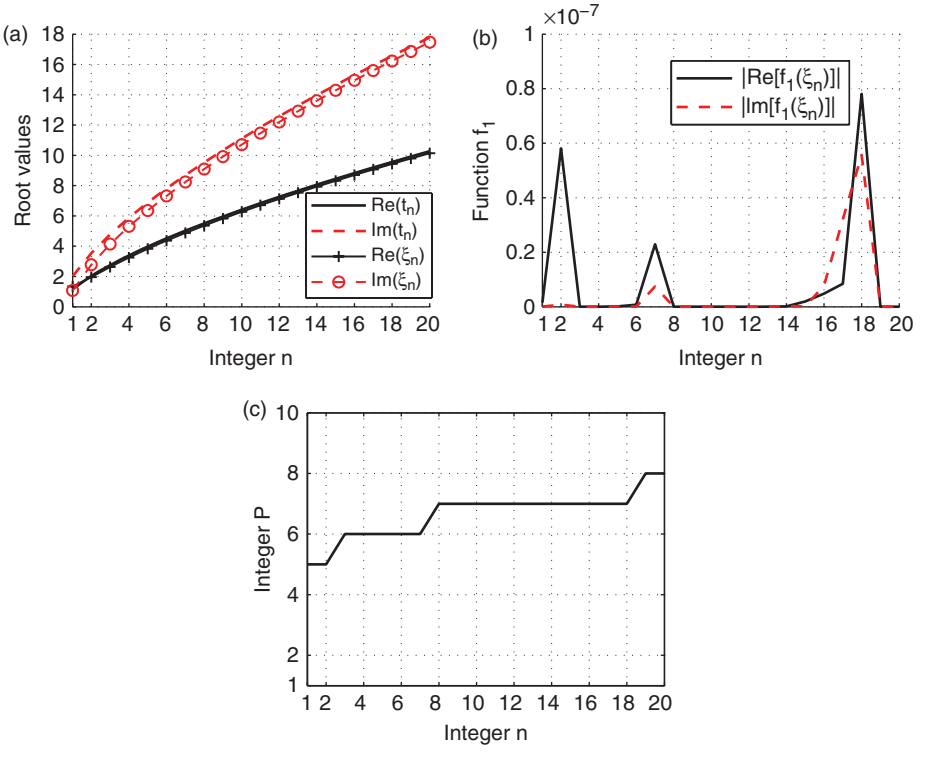

Figure 12. (Color online) (a) Root values $\{t_n, \xi_n\}$ versus the integer n. (b) Values of $f_1(\xi_n)$ versus the integer n. (c) Integer P versus the integer n. $f = 10\,\mathrm{MHz}$ and $\epsilon = 10^{-7}$.

First, the roots of Equation (11) are computed for $|q| \to \infty \Rightarrow |\Delta| \to \infty$, which leads, from fundamental properties of the Airy functions, to finding the zeros of $\mathrm{Ai}(t_n) = 0$. Letting $z_n = t_n e^{-j\pi/3}$, the roots for $|q| \to \infty$ are then expressed as $\mathrm{Ai}(-z_n) = 0$, in which z_n is real and positive. They can be computed from [15]. For instance, $z_n = \{2.3381, 4.088, 5.521, 6.787, 7.944, \ldots\}$.

For a *given* integer n, the roots of $w_1'(\xi) - qw_1(\xi) = 0$, in which $w_1(\xi) = \mathrm{Bi}(\xi) + j\mathrm{Ai}(\xi)$, can then be computed from the following recurrence equation

$$\xi_{p+1} = \xi_p - \frac{w_1'(\xi_p) - qw_1(\xi_p)}{\xi_p w_1(\xi_p) - qw_1'(\xi_p)} \quad \text{where } \xi_1 = t_n + 1/q. \tag{45}$$

The above equation was obtained from the Newton–Raphson method and from the property $w_1''(\xi) - \xi w(\xi) = 0$. The algorithm is stopped when $|f_1(\xi_p)| = |w_1'(\xi_p) - qw_1(\xi_p)| \leq \epsilon$, where ϵ is the desired precision, giving $P = p$.

For $f = 10\,\mathrm{MHz}$ and $\epsilon = 10^{-7}$, Figure 12 plots the root values $\{t_n, \xi_n\}$, the values of $f_1(\xi_n)$ and the integer P versus the integer n. As can be seen in Figure 12(c), the algorithm converges rapidly (after eight iterations) and the desired precision is reached since $|f_1(\xi_n)| < \epsilon$ in Figure 12(b). In addition, in Figure 12(a) the roots ξ_n weakly differ from the t_n roots, which explains why the algorithm converges rapidly.